



# Independent component analysis approach to image sharpening in the presence of atmospheric turbulence

Ivica Kopriva <sup>a,\*</sup>, Qian Du <sup>b</sup>, Harold Szu <sup>a</sup>, Wasyl Wasylkiwskyj <sup>a</sup>

<sup>a</sup> Department of Electrical and Computer Engineering, The George Washington University, 801 22nd Street NW, Washington, DC 20052, USA

<sup>b</sup> Department of Electrical Engineering and Computer Science, Texas A&M University-Kingsville, Kingsville, TX 78363, USA

Received 24 November 2003; received in revised form 22 December 2003; accepted 13 January 2004

## Abstract

An independent component analysis (ICA) approach to image sharpening is presented for incoherent imaging through weak atmospheric turbulence. Taking account of the turbulence model a novel data representation scheme is used for the ICA algorithm wherein each selected image frame is treated as a sensor. The proposed concept enables one diffraction limited object image and several images that correspond to atmospheric turbulence patterns to be extracted as separate physical sources. By using an image sharpening metric based on the Laplacian operator, it is shown that the ICA algorithm when applied to experimental data with known ground truth gives better results than obtained by the frame averaging method.

© 2004 Elsevier B.V. All rights reserved.

PACS: 47.27S; 42.68.B; 42.30.W; 84.35

Keywords: Atmospheric turbulence; Image sharpening; Independent component analysis; Neural networks

## 1. Introduction

The classical limit on performance of an imaging system is set by diffraction [1–3]. In accordance with the Rayleigh resolution criterion, the smallest linear dimension that can be resolved is given by

$$\delta_{X_{\text{RES}}} = 1.22 \frac{\lambda f}{B}, \quad (1)$$

where  $\lambda$  is the wavelength,  $f$  is the focal length of the lens, and  $B$  is the system aperture size. While resolution beyond the classical diffraction limit may be possible in certain cases [1,4,5] random fluctuations of the refractive index in space and time [14,15] caused by atmospheric turbulence will generally degrade the performance much beyond the classical Rayleigh diffraction limit. One way to sharpen the image is to use the frame averaging technique described in [14]. In this paper we describe a new approach to image sharpening for incoherent imaging by incorporating the physical turbulence model into the processing algorithm.

\* Corresponding author. Tel.: +1-202-994-5508; fax: +1-202-994-5171.

E-mail address: [ikopriva@gwu.edu](mailto:ikopriva@gwu.edu) (I. Kopriva).

The image sequence is processed by using the ICA algorithm [6] and treating each frame of the video sequence as a sensor. Each turbulence spatial pattern is treated as one physical source and the diffraction limited image of the original object as another source. The physical justification of the adopted data model is based on propagation of the incoherent electromagnetic waves through turbid media, as described in Section 3. After a concise account of the ICA algorithm based on fourth-order (FO) statistics in Section 4, the proposed image processing technique is detailed in Section 5. The image performance evaluation employs the Laplacian operator and is carried out for the original frames, the ICA extracted source image of the object of interest, and for a frame obtained by averaging selected frames as well as for the average of all the frames present in the image sequence [15,16]. The concluding remarks are set forth in Section 6.

## 2. Problem formulation

Inspired by the concept presented in [10], we have formulated a novel way of representing the image sequence in the ICA framework. The underlying hypothesis is similar to that used in the analysis of multispectral and/or hyperspectral data [11,12], where ICA methods are applied to a multispectral/hyperspectral image cube under the assumption of hidden sources with different spectral signatures. In the ICA framework each spectral component is treated as a sensor, as illustrated in Fig. 1(a). The same image cube con-

cept can be used to represent a temporal image sequence in the ICA framework where each frame is treated as a sensor. We do this by replacing the frequency variable ( $\omega$ ) with the time variable ( $t$ ) resulting in the temporal sequence in Fig. 1(b). It is assumed that the image sequence is acquired with a single camera and that motion effects, if present, are compensated by employing some form of image registration technique. The important novelty of this data representation scheme is that it uses the temporal information of the image sequence. The intensity variation of the (temporally) incoherent objects in time is what makes the measurements linearly independent. The underlying assumption is that different sources will have different (statistically independent) spatial realizations. This represents the basis for the image sharpening through the extraction of the spatial turbulence patterns as separate physical sources. We presume the standard linear scalar data model with additive noise

$$\mathbf{I}_i = \mathbf{A}\mathbf{I}_0 + \mathbf{v}, \quad (2)$$

where  $\mathbf{I}_i \in R^{N \times T}$  is an  $N$ -dimensional data vector (intensity in the image plane) consisted of  $T = p \times q$  samples, where  $p$  and  $q$  are frame dimensions,  $\mathbf{A} \in R^{N \times N}$  is an unknown mixing matrix,  $\mathbf{I}_0 \in R^{N \times T}$  is an unknown vector of source signals/images (intensity in the object pane), and  $\mathbf{v} \in R^{N \times T}$  represents temporally independent additive sensor noise assumed to be Gaussian. Individual components of the data vector  $\mathbf{I}_i$  are represented by  $I_{ik}(t_k, x, y)$ , where  $t_k$  is video frame index and  $(x, y)$  are pixel coordinates of the related video frame. On the component level, (2) can be written as

$$I_{ik}(t_k, x, y) = \sum_{n=1}^N a_{kn}(\Delta t_{kn}) I_{0n}(t_0, x, y). \quad (3)$$

The interpretation of (3) is that each measured data point at spatial coordinate  $(x, y)$  is a superposition of different source signals that exist at the same spatial coordinate  $(x, y)$  at some reference time  $t_0$ . The relative contributions of the individual turbulence patterns between some time  $t_k$  and the reference time  $t_0$  are contained in the unknown mixing matrix coefficients  $a_{kn}$ . One of the source components corresponds to our object of interest while the rest are different spatial realizations of

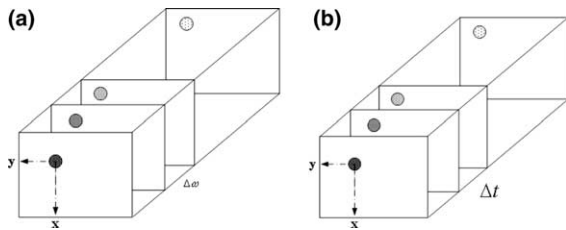


Fig. 1. (a) Representation of multispectral/hyperspectral data for ICA analysis using the concept of an image cube; (b) Using the same concept image sequence can be represented in the ICA framework where each frame is treated as a sensor.

turbulence. In the following section we provide a physical justification for this model.

### 3. Derivation of the ICA data model

A quasi-monochromatic electromagnetic field in the object plane is transformed into its image (Figs. 2 and 3) by the superposition integral (extended Huygens–Fresnel principle) [1,3,13,14]

$$\hat{U}_i(\alpha_2) = \int d\alpha_1 U_o(\alpha_1) p_l(\alpha_2, \alpha_1), \quad (4)$$

where  $\alpha_i = \rho_i/L$  is the angular coordinate,  $L$  is the atmospheric path length,  $\hat{U}_i$  represents the electromagnetic field after the imaging lens,  $U_o$  is electromagnetic field in the object plane and

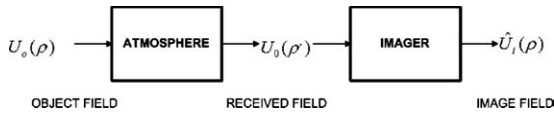


Fig. 2. Block diagram of a general atmospheric imaging system, taken from [14].

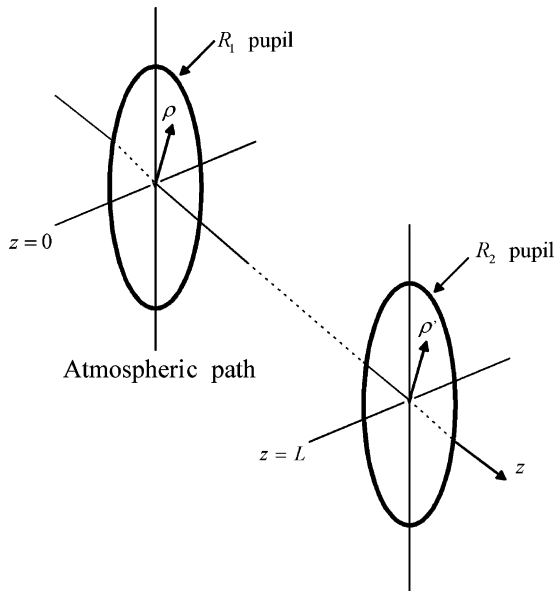


Fig. 3. Line of sight propagation geometry, taken from [14].

$p_l(\alpha_2, \alpha_1)$  is the system point spread function which may be represented by

$$p_l(\alpha_2, \alpha_1) = \lambda^{-2} \int_{R_2} d\rho' \exp \{ \chi(\rho', \alpha_1 L) + i[\Phi(\rho', \alpha_1 L) + k\rho'(\alpha_2 - \alpha_1)] \}, \quad (5)$$

where  $k = 2\pi/\lambda$  is the wave number,  $\lambda$  is the wavelength,  $\chi(\rho', \alpha_1 L)$  and  $\Phi(\rho', \alpha_1 L)$  are log amplitude and phase of the atmospheric turbulence in the image plane and the integration is carried out over the pupil  $R_2$  in Fig. 3. If pupil in the object plane lies within a single atmospheric coherence area, (4) can be replaced by

$$\hat{U}_i(\alpha_2) = \int d\alpha_1 U_o(\alpha_1) p_l(\alpha_2 - \alpha_1), \quad (6)$$

while the point spread function (5) simplifies to [13]

$$p_l(\alpha) = \lambda^{-2} \int_{R_2} d\rho' \exp \{ \chi(\rho', 0) + i[\Phi(\rho', 0) + k\rho'\alpha] \}. \quad (7)$$

For the incoherent electromagnetic fields, the optical intensity in the image plane is given by

$$\begin{aligned} \hat{I}_i(\alpha_2, t) &= \langle U_i(\alpha_2, t) U_i^*(\alpha_2, t) \rangle \\ &= \int d\alpha_1 L^{-2} A_s \langle U_o(\alpha_1, t) U_o^*(\alpha_1, t) \rangle |p_l(\alpha_2 - \alpha_1)|^2 \\ &= \int d\alpha_1 L^{-2} A_s I_o(\alpha_1, t) |p_l(\alpha_2 - \alpha_1)|^2, \end{aligned} \quad (8)$$

where  $A_s$  is the source coherence area and  $I_o(\alpha_1, t)$  is optical intensity in the object plane at the angular coordinate  $\alpha_1$ . If point source is assumed

$$I_o(\alpha_1, t) = I_o(t) \delta(\alpha - \alpha_1), \quad (9)$$

so that (8) reduces to

$$\hat{I}_i(\alpha_2, t) = I_o(t) L^{-2} A_s |p_l(\alpha_2)|^2. \quad (10)$$

Both the log-amplitude and the phase of the atmospheric turbulence can be rewritten as

$$\begin{aligned} \chi(\rho', 0, t) &= \Delta\chi(\rho', 0, t) + \chi(\rho, 0, t_0), \\ \Phi(\rho', 0, t) &= \Delta\Phi(\rho', 0, t) + \Phi(\rho, 0, t_0), \end{aligned} \quad (11)$$

where  $t_0$  is a reference time, and  $\chi(\rho, 0, t_0)$  and  $\Phi(\rho, 0, t_0)$  are reference values of the log amplitude and phase of the atmospheric turbulence in the object plane. This is in agreement with the Taylor's frozen hypothesis [14] which states that change of

the refractive index over short time interval  $t > t_0$  remains fixed except for translation with the uniform velocity with components  $v_x$ ; and  $v_y$ . We then have

$$n_m(x, y, t) = n_m[x - v_x(t - t_0), y - v_y(t - t_0), t_0], \quad (12)$$

where index  $m$  corresponds with the particular source of turbulence. Based on (11), (7) can be written as a function of time as

$$p_l(\alpha, t) = \exp(\Delta\chi(\rho', 0, t) + i\Delta\Phi(\rho', 0, t))p_l(\alpha, t_0), \quad (13)$$

which gives

$$|p_l(\alpha, t)|^2 = \exp(2\Delta\chi(\rho', 0, t))|p_l(\alpha, t_0)|^2. \quad (14)$$

The interpretation of (11) and (12) is that the sources of turbulence can be placed at some reference temporal location  $(\rho, t_0)$  so that the relative atmospheric turbulence contribution in both log-amplitude and phase for some time  $t > t_0$  is taken into account by (11). Under this assumption, we can rewrite (10) for the case when at detector location  $\alpha_2$ , in addition to the source signal that comes from the object itself, several other source signals, corresponding to different atmospheric turbulence patterns along the atmospheric path, arrive. The optical intensity

$$I_i(\alpha_2, t) = \sum_{n=1}^N I_{on}(t_0)L^{-2}A_{sn} \times \exp[2\Delta\chi(\rho'_n, 0, t)]|p_l(\alpha_2, t_0)|^2 \quad (15)$$

can be identified with  $I_{ik}(\alpha, t_k)$  in the adopted ICA data model (2) and (3)

$$I_{ik}(\alpha, t_k) = \sum_{n=1}^N a_{kn}I_{on}(\alpha, t_0) + v_k(\alpha, t_k), \quad (16)$$

where we have used the angular coordinates and assumed that the additive noise term  $v_k(\alpha, t_k)$  is Gaussian. The source vector components and mixing matrix components are identified from (15) and (16) as

$$a_{kn} = L^{-2}A_{sn} \exp[2\Delta\chi(\rho'_n, 0, t_k)], \quad (17)$$

$$I_{on}(\alpha, t_0) = I_{on}(t_0)|p_l(\alpha, t_0)|^2.$$

Evidently the reconstructed image  $\hat{I}_{on}(\alpha, t_0)$  is affected by the point spread function. However, if uniform weighting is assumed, i.e.,  $|p_l(\alpha_1, t_0)|^2 \cong |p_l(\alpha_2, t_0)|^2$ , the reconstructed image will be a scaled version of the original object image, which amounts to standard indeterminacy inherent in ICA algorithms [6].

#### 4. The fourth-order statistics-based ICA algorithm

Strategy of ICA algorithms is to find a linear transformation  $\mathbf{W}$

$$\hat{\mathbf{I}}_o = \mathbf{W}\mathbf{I}_i = \mathbf{W}\mathbf{A}\mathbf{I}_o + \mathbf{W}\mathbf{v} = \mathbf{Q}\mathbf{I}_o + \mathbf{W}\mathbf{v}, \quad (18)$$

such that the components of the vector  $\hat{\mathbf{I}}_o$  are as statistically independent as possible. Based on the assumption that the source signals  $I_{on}$  are mutually statistically independent and non-Gaussian (except maybe one), the vector  $\hat{\mathbf{I}}_o$  will represent the source signals  $\mathbf{I}_o$  within a permutation and a scale factor. Here, we are going to use the FO cumulant-based ICA algorithm JADE (joint approximate diagonalization of the eigen-matrices) [6], wherein statistical independence is achieved through the minimization of the squares of the FO cross-cumulants among the components of  $\hat{\mathbf{I}}_o$

$$\mathbf{W} = \arg \min \sum_m \sum_l \sum_k \sum_j \mathbf{off}(\mathbf{W}^T \hat{C}(I_{ij}, I_{ik}, I_{il}, I_{im}) \mathbf{W}), \quad (19)$$

where the operation  $\mathbf{off}(\mathbf{A})$  on a matrix  $\mathbf{A}$  is represented by

$$\mathbf{off}(\mathbf{A}) = \sum_{1 \leq i \neq j \leq N} |a_{ij}|^2 \quad (20)$$

and the  $\hat{C}(I_{ij}, I_{ik}, I_{il}, I_{im})$  are sample estimates of the fourth-order cross-cumulants [7,8] defined by

$$\begin{aligned} \hat{C}(I_{ij}, I_{ik}, I_{il}, I_{im}) = & E[I_{ij}I_{ik}I_{il}I_{im}] - E[I_{ij}I_{ik}]E[I_{il}I_{im}] \\ & - E[I_{ij}I_{il}]E[I_{ik}I_{im}] - E[I_{ij}I_{im}]E[I_{ik}I_{il}], \end{aligned} \quad (21)$$

where  $E[\cdot]$  denotes mathematical expectation. The additional advantage of using a FO cumulant-based ICA algorithm is its capability to suppress additive Gaussian noise since FO cumulants are blind with respect to Gaussian noise [7]. Based on

the multilinearity property of cumulants [7,8], we can write any of the FO cross-cumulants as follows:

$$C(I_{ij}, I_{ik}, I_{il}, I_{im}) = \sum_{n=1}^N q_{jn} q_{kn} q_{ln} q_{mn} C_4(I_{on}) + \sum_{n=1}^N w_{jn} w_{kn} w_{ln} w_{mn} C_4(v_n). \quad (22)$$

For Gaussian noise, the last term vanishes identically so that (22) simplifies to

$$C(I_{ij}, I_{ik}, I_{il}, I_{im}) \cong \sum_{n=1}^N q_{jn} q_{kn} q_{ln} q_{mn} C_4(I_{on}). \quad (23)$$

A critical factor in ICA applications is the level of (non)-singularity of the mixing matrix  $\mathbf{A}$ . Although the mixing matrix is unknown, we must assume it to be invertible. In the proposed image sharpening application it is affected by the selection of time displacement  $\Delta t$  between the video frames used as sensors in the ICA data model (2) and (3). The video frames incorporated into the ICA data model must be sufficiently different so that the measurements are linearly independent. It seemed natural to use the Kullback–Leibler divergence to measure the mutual information between the images  $\mathbf{p}$  and  $\mathbf{q}$  [9]

$$D(\mathbf{p}, \mathbf{q}) = L(\mathbf{p}; \mathbf{q}) + L(\mathbf{q}; \mathbf{p}), \quad (24)$$

$$L(\mathbf{p}; \mathbf{q}) = \sum_{k=1}^T p_k \frac{p_k}{q_k}, \quad L(\mathbf{q}; \mathbf{p}) = \sum_{k=1}^T q_k \frac{q_k}{p_k}, \quad (25)$$

where  $p_k$  and  $q_k$  are pixel intensities at the spatial coordinate  $k \cong (x, y)$ . Because the Kullback distance is not symmetrical both distances  $L(\mathbf{p}; \mathbf{q})$  and  $L(\mathbf{q}; \mathbf{p})$  are used in (24). When two images are the same the Kullback distance  $D(\mathbf{p}, \mathbf{q})$  will be zero, i.e., the mutual information will be maximum, implying that the mutual information is inversely proportional to the Kullback distance. When a predefined number of frames is randomly selected from the set of frames that correspond to the image sequence, the mutual information between them is measured in order to ensure that selected frames represent linearly independent measurements.

## 5. Experimental results

In order to verify the proposed image sharpening technique we have used an image sequence of the Washington monument. The image sequence contained 50 frames. Fig. 4 illustrates for three randomly selected frames how the ICA algorithm extracts one diffraction limited source image that corresponds to the original object and the two extracted source images that correspond to the spatial turbulence patterns. Fig. 4(a) shows three frames randomly selected from the 50 frames. In the ICA context these frames are called data frames. Fig. 4(b) shows the extracted source images using the JADE algorithm [6]. As expected, one source image corresponds to the original object and other two source images correspond to turbulence realizations. As discussed in [14,15] the

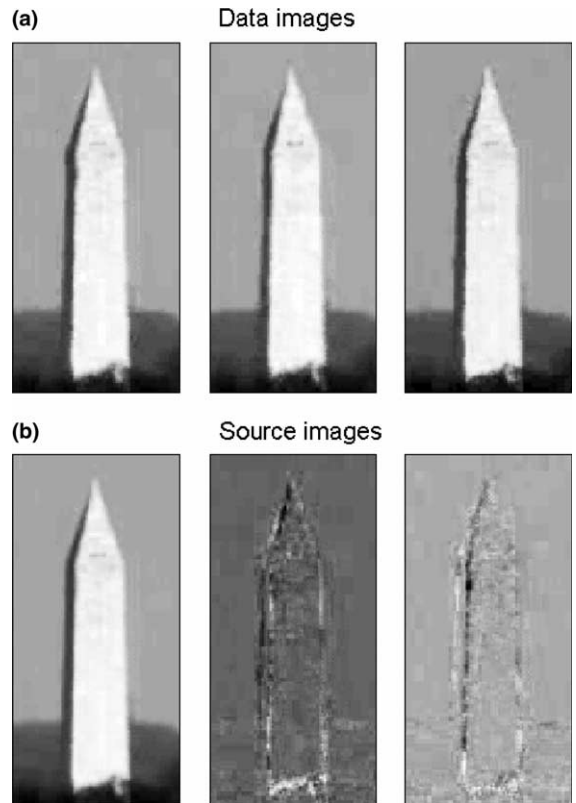


Fig. 4. (a) Three data frames randomly selected from the 50 frames that form the image sequence; (b) Extracted source images using JADE ICA algorithm [6].

image distortion caused by turbulence can also be reduced by a frame averaging method. However, it is known that the frame averaging approach suffers from a loss of details. This is not the case with the proposed algorithm. Fig. 6 shows, from left to right, images obtained by averaging two and three randomly selected frames as well as by averaging all 50 frames contained in the image sequence. In order to quantify the performance of the proposed image sharpening approach we have used a metric based on the Laplacian operator [17]. The Laplacian operator approximates the linear second derivative of intensity  $I_{ik}$  in direction  $x$  and  $y$

$$S(x, y) = \nabla^2 I_{ik}(x, y) \equiv \frac{\partial^2 I_{ik}(x, y)}{\partial x^2} + \frac{\partial^2 I_{ik}(x, y)}{\partial y^2}, \quad (26)$$

and the image sharpening metric is defined by

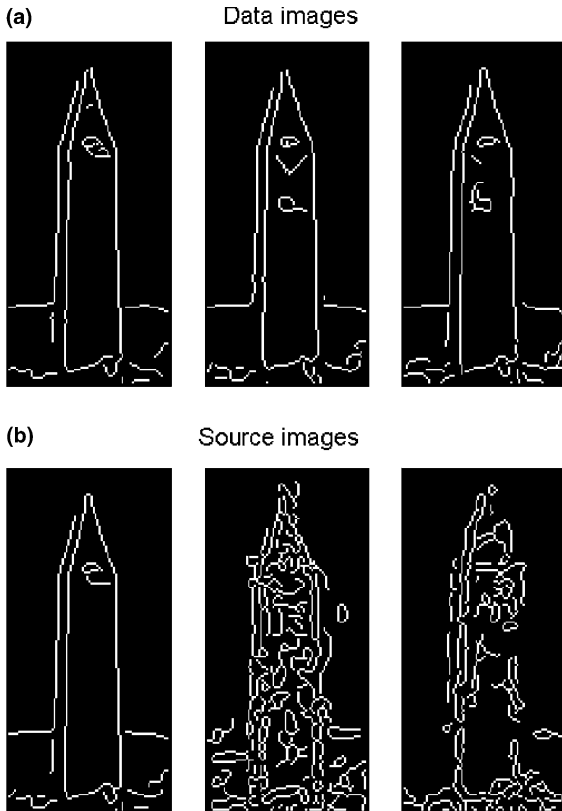


Fig. 5. (a) Edges extracted by the Canny's method for three data frames shown in Fig. 4(a). (b) Edges extracted by the Canny's method for three source images shown in Fig. 4(b).

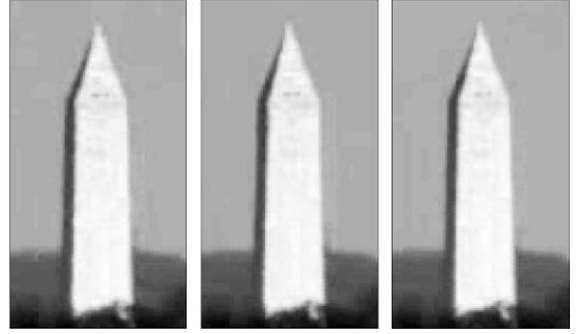


Fig. 6. From left to right: images obtained as an average of 2, 3, and 50 frames.

$$S_4 = \frac{1}{qp} \sum_x \sum_y |S(x, y)|, \quad (27)$$

where  $q$  and  $p$  represent image dimensions in  $x$  and  $y$  directions, respectively. The proposed metric is equivalent to the image sharpening metric in [17,14] defined by

$$S_4^* = \frac{1}{qp} \int \int \left| \frac{\partial^4 I_{ik}(x, y)}{\partial x^2 \partial y^2} \right| dx dy. \quad (28)$$

What makes (27) suitable as a performance measure is that the Laplacian operator is inherently a spatial high-pass filter, so that it yields a larger response to a line than to a step, and also to a point than to a line [17]. An image that contains turbulence is typically comprised of points varying in brightness, and the Laplacian operator will emphasize the points. In that sense the extracted source image that corresponds to the original object should have the smallest value of the metric  $S_4$  compared with both the original data images and the extracted source images that correspond to the turbulence patterns. Table 1 gives values of the metric (27) for the three images shown in Fig. 6. They were obtained by averaging two and three randomly selected frames as well as by averaging all 50 frames. Results shown in Table 1 are in agreement with the known fact that the noise variance is decreased when number of observations (i.e., frames) is increased. This confirms the consistency of the adopted image sharpening metric (27). As expected, the smallest value of metric (27) is obtained for averaging all 50 frames. Table

Table 1

Image enhancement metric (27) obtained for the four images obtained as an average of two, three, four randomly selected frames as well as an average of all 50 frames

Number of the averaged frames	2	3	50
The sharpening metric $S_4$	8.6698	8.5572	8.2468

2 gives results for the metric  $S_4$  for both data and source images for two randomly selected frames. As expected, the source image  $\hat{I}_{o1}$  that corresponds to the original object has the smallest value of the metric  $S_4$  when compared with both data images  $I_{i1}$  and  $I_{i2}$  as well as with the averaged image (the first image on the left in Fig. 6) whose metric is given in the second column of Table 1. We also want to comment that the metric  $S_4$  associated with the source image  $\hat{I}_{o1}$  is smaller than values obtained from the averaged images given in Table 1. The same conclusion applies in the case of the three randomly selected sources illustrated in Fig. 4 for which the value of metric  $S_4$  is given in Table 3. This suggests that by using the proposed approach better image sharpening results can be obtained by randomly selecting a small number of frames (two or three) than by averaging a large number of frames (50 in this case). This result is also important due to the fact that the frame averaging approach to image sharpening has as a side effect the tendency to produce images with loss of details, which is

Table 2

Image enhancement metric (27) obtained for two randomly selected frames as well as for the corresponding two source images extracted by JADE ICA algorithm [6]

Image	$I_{i1}$	$I_{i2}$	$\hat{I}_{o1}$	$\hat{I}_{o2}$
The sharpening metric $S_4$	9.177	8.9569	8.1743	11.9205

Table 3

Image enhancement metric (27) obtained for three randomly selected frames as well as for the corresponding three source images extracted by JADE ICA algorithm [6]

Image	$I_{i1}$	$I_{i2}$	$I_{i3}$	$\hat{I}_{o1}$	$\hat{I}_{o2}$	$\hat{I}_{o3}$
The sharpening metric $S_4$	9.1051	9.0119	9.3600	8.0625	14.3057	13.564

not the case with the approach proposed here. As expected, metric  $S_4$  obtained for the source images associated with the turbulence patterns has the greatest value by comparison with both the original data images as well as with images obtained by the frame averaging method. To further illustrate the performance of the proposed image sharpening algorithm we have shown in Fig. 5(a) edges extracted by the Canny’s method for the three randomly selected frames as shown in Fig. 4(a), and in Fig. 5(b) edges for the three extracted source images as shown in Fig. 4(b). As could be seen from the leftmost image in Fig. 5(b), details like windows, the boundary line between the vertical flat and inclined pyramidal face as well as the top of the monument are reconstructed. That is not the case with the raw data images shown in Fig. 4(a) the edges of which are shown in Fig. 5(a), where on some data images the top of monument is not reconstructed, the boundary line is missed on all of them or turbulence artifacts are present on the vertical flat face of the monument. To further characterize turbulence we have estimated scintillation index calculated as the normalized variance of the irradiance fluctuations [13]

$$\beta^2 = \frac{\langle I_{ik}^2 \rangle - \langle I_{ik} \rangle^2}{\langle I_{ik} \rangle^2}. \tag{29}$$

The results are given in Table 4 for the three data images shown in Fig. 4(a). The value of the scintillation index is approximately 0.02. Accordingly the atmospheric turbulence present in the image sequence presented herein can be classified as a weak.

Table 4

Scintillation index for the three data images shown in Fig. 4(a)

Image	$I_{i1}$	$I_{i2}$	$I_{i3}$
Scintillation index	0.0192	0.0199	0.0197

## 6. Conclusion

A novel approach to the image sharpening in the presence of atmospheric turbulence is proposed in this paper which is based on the application of the ICA algorithm to randomly selected frames from the image sequence. The mutual information between the selected image frames was measured in order to ensure linearly independent measurements. In the ICA framework, the selected frames were used as sensors implying that the underlying sources are spatially independent. We have demonstrated the capability of the proposed concept to extract blurring effects contributed by atmospheric turbulence as separate physical sources. A metric based on the Laplacian operator is employed to quantify the performance. Comparison is made among the original data images, image obtained by the frame averaging method and diffraction limited object source images extracted by the ICA algorithm for the case of two and three selected frames. The best results were always obtained for the ICA extracted object image when compared to both the original data images and images obtained by the frame averaging method. Unlike the frame averaging method, the proposed ICA approach does not suffer from loss of detail. Based on the value of the estimated scintillation index, the turbulence present in the experimental data is classified as weak.

## References

- [1] J.W. Goodman, *Introduction to Fourier Optics*, second ed., McGraw-Hill, New York, 1996, p. 63.
- [2] M. Born, E. Wolf, *Principles of Optics*, sixth ed., Cambridge, 1980, p. 491.
- [3] J.W. Goodman, *Statistical Optics*, Wiley, New York, 1985, p. 157.
- [4] A.W. Lohman, D. Mendlovic, *J. Opt. Soc. Am. A* 14 (1997) 558.
- [5] H. Szu, I. Kopriva, *Opt. Commun.* 198 (1–3) (2001) 71.
- [6] J.F. Cardoso, A. Souloumiac, *IEE-Proc. F* 140 (1993) 362.
- [7] J.M. Mendel, *Proc. IEEE* 79 (1991) 278.
- [8] P. McCullagh, *Tensor Methods in Statistics*, Chapman & Hall, London, 1987, 1995, p. 24.
- [9] C. Thomas, *Elements of Information Theory*, Wiley-Interscience, New York, 1991.
- [10] I. Schiefl, M. Stetter, J.E. Mayhew, N. McLoughlin, J.S. Lund, K. Obermayer, *IEEE Trans. Biomed. Eng.* 47 (2000) 573.
- [11] L. Parra, C. Spence, P. Sajda, A. Ziehe, K-R. Müller, in: S.A. Jolla, T.K. Leen, K-R. Müller (Eds.), *Advances in Neural Information Processing Systems 12 (NIPS12)*, MIT Press, Cambridge, 2000, p. 942.
- [12] H.H. Szu, C. Hsu, *Proc. SPIE* 3078 (1997) 147.
- [13] J.H. Shapiro, in: J. Strohbehm (Ed.), *Laser Beam Propagation in the Atmosphere*, Topics in Applied Physics, 25, Springer, New York, 1978, p. 171.
- [14] M.C. Roggemann, B. Welsh, *Turbulence Effects on Imaging Systems*, CRC Press, Boca Raton, 1996, p. 57.
- [15] M.C. Roggemann, D.W. Tyler, M.F. Bilmont, *Appl. Opt.* 31 (1992) 7429.
- [16] R.A. Muller, A. Buffington, *J. Opt. Soc. Am.* 64 (1974) 1200.
- [17] J.C. Russ, *The Image Processing Handbook*, CRC Press, Boca Raton, 1992, p. 101.